

Green synthesis, characterization and applications of TiO₂ nanoparticles using aqueous extract of *Erythrina variegata* leaves

Jayaram Mari Selvi¹, Mariappan Murugalakshmi^{1,*}, Ponnusamy Sami²,
Mariappan Gnanaprakash³ and R. Thanalakshmi¹

¹PG & Research Department of Chemistry, The Standard Fireworks Rajaratnam College for Women, Sivakasi 626 123, India

²PG & Research Department of Chemistry, Virudhunagar Hindu Nadar's Senthikumara Nadar (VHNSN) College, Virudhunagar 626 001, India

³Mepco School of Management Studies, Mepco Schlenk Engineering College (Autonomous), Sivakasi 626 001, India

Green synthesis is a simple, non-toxic, economical and eco-friendly approach for the synthesis of nanoparticles (NPs). The implementation of new technologies has led to the new area of nano revolution which unfolds the role of plants in bio- and green synthesis of nanomaterials. The plant extracts employed are neem, lemon grass, aloe vera, Indian gooseberry, etc., focusing on the green chemistry principles. In the present work, NPs of titanium dioxide (TiO₂) were synthesized using an aqueous extract of *Erythrina variegata* leaves as a capping agent. The leaf extract was utilized as a reducing agent for the conversion of metal precursors into metal-oxide NPs. *E. variegata*-mediated TiO₂ NPs were characterized by UV-Vis absorption spectroscopy, Fourier transform infrared spectroscopy, X-ray diffraction (XRD), energy-dispersive X-ray spectroscopy and morphological studies were conducted by scanning electron microscopy. The UV-Vis absorption spectrum showed an absorption band at 317.6 nm, which supports the formation of TiO₂ NPs. The optical band-gap energy was determined to be 2.35 eV. Further characterization by XRD supported the crystallinity and purity of the synthesized TiO₂ NPs. These NPs may have effective dye degradation ability. The green-synthesized TiO₂ NPs exhibited interesting photocatalytic efficacy on methylene blue dye under UV irradiation (using a multi-lamp photo reactor) and antibacterial activity against pathogenic organisms like *Streptococcus*, *Staphylococcus*, *Escherichia coli* and *Pseudomonas aeruginosa*.

Keywords: Antibacterial activity, *Erythrina variegata*, green synthesis, nanoparticles, photocatalytic efficacy, titanium dioxide.

In the last few years, nanoparticles (NPs) have gained importance in the scientific field due to their typical size, shape, surface area and technological applications like

electrical, optical, magnetic, catalytic, biomedical and antibacterial activities which cannot be achieved by their bulk counterparts¹⁻⁹. Several traditional synthetic methods have been developed by various research groups to synthesize NPs using physico-chemical methods^{10,11}.

NPs are defined as a cluster of atoms between 1 and 100 nm in size that behave like a whole unit with respect to all their properties¹². NPs are one of the most important gifts of science in the modern era. Nanotechnology mainly deals with the synthesis of NPs of variable size, shape, chemical composition and their potential use for the benefit of humanity¹³. The preparation of NPs can be done under three main conditions: (i) choice of environment-friendly solvent medium, (ii) reducing agent and (iii) a non-toxic material for their stabilization¹⁴. NPs are the building blocks of the next generation of technology with applications in several other fields¹⁵.

Nanotechnology is an important branch of science. It deals with the synthesis and development of various types of NPs in sizes ranging from 1 to 100 nm (ref. 16). It has been noted that the physical and chemical properties of any material change when its size decreases to nanoscale^{17,18}. The characteristics depend on certain traits such as size, particle distribution, morphology and high surface/volume ratio¹⁹. Metal-oxide NPs have gained attention for their potential applications in optoelectronics, nanodevices, nanoelectronics, nanosensors, information storage and catalysis²⁰. Various metal-oxide NPs have been implemented in a wide range of applications. They can be used as catalysts in reduction, oxidation electrocatalysis, photocatalysis and gas-phase reactions²¹.

Green synthesis is eco-friendly and manufactures stable and multiuse nanomaterials which involves on the action of biomolecules and works as a reducing and capping agent without toxicity, and supports the ease in manufacturing. The physical and chemical techniques are cost-effective and they involve the usage of instruments or chemical agents. Another limitation is low stability, contamination with residuals of agents and less compatibility in the pharmaceutical and cosmetics industry^{22,23}. Moreover,

*For correspondence. (e-mail: m_murugalakshmi@yahoo.com)

plant leaf extracts are the best candidates for the synthesis of NPs.

In the present study, the leaf extract of *Erythrina variegata* belonging to the family Fabaceae, commonly known as 'Kalyana murungai', was chosen. It has high medicinal value and properties. *E. variegata* possesses distinctive biological actions, including antibacterial/dental caries prevention, CNS effects, cardiovascular effects, antioxidant, smooth muscle relaxant, analgesic and anti-inflammatory, calcium homeostasis, trypsin/proteinase inhibitors and cytotoxicity²⁴. Its leaves have metal and salt-reducing properties. *E. variegata* has been used in traditional medicine as a nervine sedative, febrifuge, anti-asthmatic and antiepileptic. The leaves are used to treat fever, inflammation and joint pain. The juice of the leaves is used to treat earache, toothache, constipation, cough, and to stimulate lactation and menstruation²⁵. The bark is used to treat fever, liver problems and rheumatism.

E. variegata contains several phenolic metabolites, such as pterocarpan, isoflavones, flavanones and chalcones, some of which display antiplasmodial, antimycobacterial and cytotoxic activity against various cancer cell lines. It also contains alkaloids like *N*-norprotosinomenine (I), dimethyltryptophan, hyparphorine and sterols like campesterol, β -sitosterol and β -amyirin. The isoflavones indicanines D and E, genistein, wightone, alpinum isoflavones, dimethyl alpinum isoflavone, 8-prenyl erythrinin C and erysenegalsein E – erythrinassinate B, apigenin, genkwanin, isovitexin, swertisin, saponarin, 5-*O*-glucosylswertisin and 5-*O*-glucosylisowertisin. Glucoside swertiamarin, a triterpene betulin have also been isolated. The alcohol insoluble portion of the unsaponifiable matter has yielded *n*-hexosamol, heptacosine, nonacosane and non-saponifiable matter of the petroleum ether extract has yielded myristic, stearic and oleic acids^{26–28}.

In this study, *E. variegata* leaf aqueous extract was used for the synthesis of TiO₂ NPs to evaluate the reduction power of this extract as a green route of TiO₂ NPs production. The effect of extract volume was studied using UV-Vis spectroscopy, Fourier transform infrared spectroscopy (FTIR), X-ray diffraction (XRD), scanning electron microscopy (SEM) and energy-dispersive X-ray spectroscopy (EDAX). Next, its application in photocatalytic degradation of methylene blue dye and antibacterial activity action on *Streptococcus*, *Staphylococcus*, *E. coli* and *Pseudomonas aeruginosa* was analysed.

Materials and methods

Plant material

Leaves of *E. variegata* were collected from the garden of The Standard Fireworks Rajaratnam College for Women, Sivakasi, Virudhunagar district, Tamil Nadu, India and dried in the shade. These were then powdered and stored in an air-tight container at room temperature until further use.

Chemicals

Titanium tetraisopropoxide (TTIP; Sigma Aldrich, AR-grade, purity >97%) was purchased from the National Scientific Company in Villapuram, Madurai, Tamil Nadu, India.

Glassware

Glassware such as conical flask, measuring cylinder, beaker, watch glass, magnetic stirrer, funnel, standard measuring flask, round-bottom flask, condenser and Soxhlet apparatus were used.

Plant extract preparation

E. variegata leaves were washed several times with water to remove dust particles. The leaves were dried in the shade at room temperature for ten days. The dried leaves were ground to a fine powder. The aqueous extract was prepared using the Soxhlet extraction method. In the Soxhlet apparatus, solvent (150 ml of distilled water) was added to a round-bottom flask, which was attached to a Soxhlet extractor and condenser on an isomantle. Then 15 g of dried leaf powder of the plant material was loaded into the thimble placed inside the Soxhlet extractor. The side arm was lagged with glass wool. The solvent was heated using the isomantle and began to evaporate at 100°C, moving through the apparatus to the condenser. The condensate drips into the reservoir containing the thimble. Once the level of solvent reached the siphon, it was poured in dropped into the flask and the cycle started again. The process should run for a total of 6 h. After 6 h of continuous extraction, the fine extract containing various natural compounds was filtered using Whatmann No. 1 filter paper and stored safely for further use.

Synthesis of TiO₂ NPs

TTIP (1 N) was prepared using distilled water and a colourless solution was obtained. Next, 20 ml of *E. variegata* extract was added to 0.1 N TTIP solution. The colour of the mixture changed from pale yellow immediately and slowly turned to sandal after 6 h of continuous stirring. This colour change is due to the formation of TiO₂ NPs. The synthesized NPs were separated by centrifuging and dried in a hot air oven at 100°C for 6 h. The NPs were characterized by UV-Vis spectrum, FTIR, XRD, SEM and EDAX studies (Figure 1).

Characterization of TiO₂ NPs

The colour change in the reaction mixture was visually examined. The absorption maxima in UV-Vis (Shimadzu

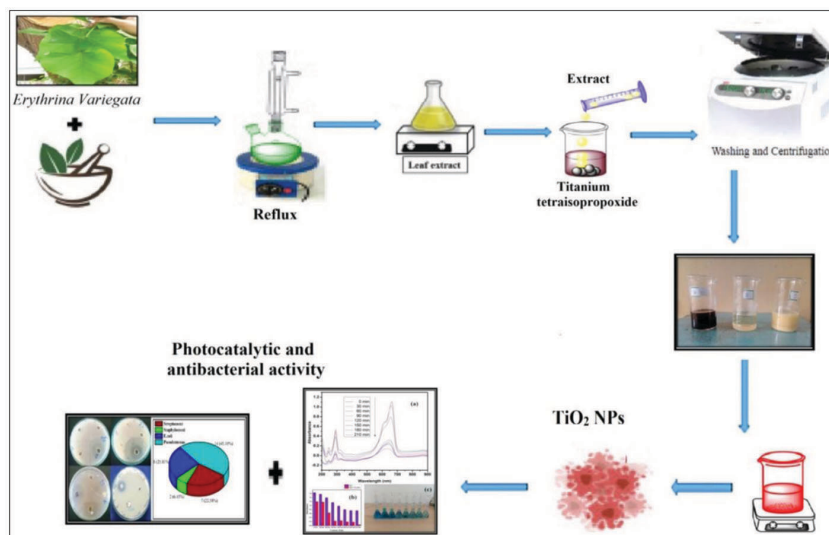


Figure 1. Schematic view of titanium dioxide (TiO₂) nanoparticles (NPs) synthesis using *Erythrina variegata* leaves.



Figure 2. Colour change indicating the TiO₂ NPs formation.

UV-2450) double-beam spectrophotometer in the range between 200 and 900 nm using distilled water as a reference. The FTIR spectrum of TiO₂ NPs was recorded (Shimadzu IR-Affinity-1 FTIR spectrophotometer, The Standard Fireworks Rajaratnam College for Women, Sivakasi, Tamil Nadu, India). The functional groups present in the samples were identified using FTIR spectral data. The sample was prepared as 0.25 mm thick KBr pellets (1 mg in 100 mg KBr). The spectrum was recorded between 4000 and 400 cm⁻¹ nm for 70 scans. XRD patterns were obtained for the powder samples (Bruker D8 advance ECO X-ray diffractometer, Kalasalingam University, Krishnankoil, Tamil Nadu, India). Phase purity and size were determined by XRD analysis. The average size of TiO₂ NPs was calculated using the Debye–Scherrer equation. The morphology and chemical composition of the synthesized NPs were examined by EDAX (6490 LA) at an acceleration voltage of 20 kV.

Photocatalytic activity of TiO₂ NPs

The photocatalytic degradation of methylene blue (chemical name (3,7 bis (dimethylamino) phenazathionium chloride tetramethylthionine chloride), MF = C₁₆H₁₈CIN₃S,

3H₂O, MW = 319.85 g/mol) solution was performed using green-synthesized TiO₂ NPs in UV light (multi-lamp photo reactor with light source @ 365 nm). In this experiment, a suspension was prepared by adding 0.02 mg of TiO₂ NPs to 100 ml of 10 ppm methylene blue solution. Then the mixture was stirred for about 30 min in darkness to ensure the constant equilibrium of TiO₂ NPs in the dye solution. Degradation was visually detected by a gradual change in the colour of the dye solution from deep blue to colourless. Simultaneously, the absorbance of dye solution before and after degradation by TiO₂ NPs at regular time intervals of exposure to UV light was measured.

Antibacterial activity of TiO₂ NPs

The antibacterial activity of *E. variegata* leaf extract-mediated TiO₂ NPs was examined using broth dilution and disc-diffusion method against pathogenic organisms like *Streptococcus*, *Staphylococcus*, *E. coli* and *P. aeruginosa*. The results were predicted based on the zone of inhibition.

Results and discussion

Visual observations

This is the primary test for checking the formation of TiO₂ NPs. The sequential colour change indicates the formation of TiO₂ NPs by the plant material. Leaf extract was added to the TTIP solution. Within 2 min, the colour changed from pale yellow to sandal. After incubation, the colour changed from pale yellow to sandal, indicating the formation of TiO₂ NPs (Figure 2).

UV-Vis spectral studies

The UV–Vis spectra of the green-synthesized TiO₂ NPs were recorded using a double-beam spectrophotometer

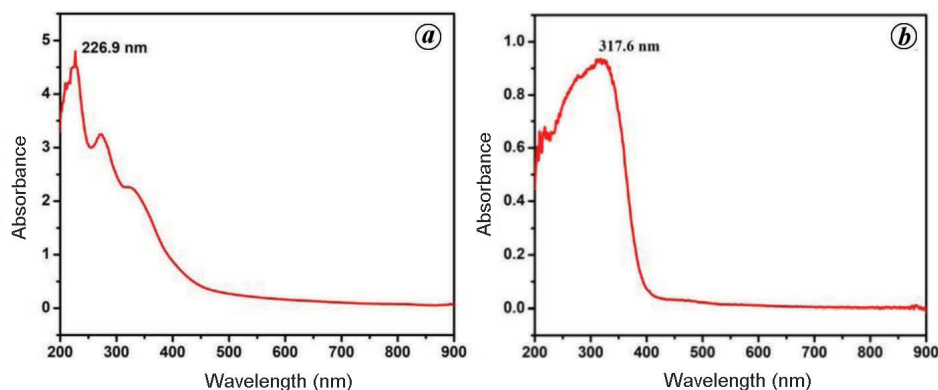


Figure 3. *a*, UV-visible spectrum of aqueous extract of *Erythrina variegata* leaves. *b*, Synthesized TiO₂ NPs.

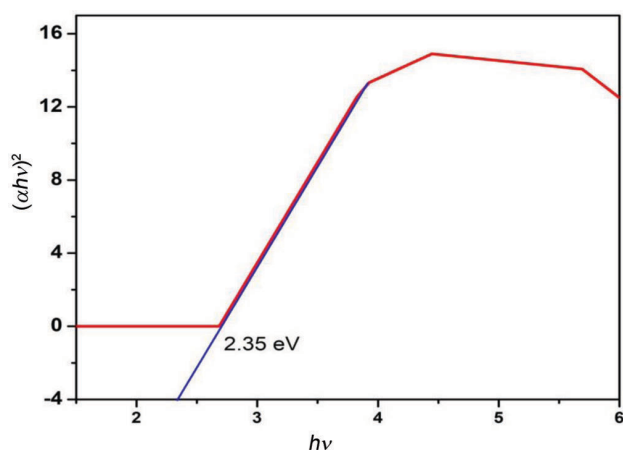


Figure 4. Tauc plot of TiO₂ NPs.

(Shimadzu UV-2450 PC) in the range 200–900 nm. Figure 3 shows the absorption spectrum of aqueous extract of *E. variegata* leaves and the synthesized TiO₂ NPs. The absorption maximum at 317.6 nm supports the formation of TiO₂ NPs (Figure 2).

Tauc plot band-gap energy calculation

The band-gap energy can be determined using the Tauc relation. The dependence of the optical band gap (E_g) on the absorption coefficient and the incident photon energy ($h\nu$) is given by the following relation

$$\alpha h\nu = A(h\nu - E_g)^n,$$

where A is the optical constant, α the absorption coefficient, h the Planck's constant, ν the frequency of the incident photon and n is the number characterizing the nature of the transition process (here $n = 2$ for direct transition and $n = 1/2$ for indirect transition). The value of E_g was obtained by plotting $h\nu$ versus $(\alpha h\nu)^2$ and then extrapolating the linear region on the energy axis (Figure 4).

The value of E_g was 2.35 eV for 317.6 nm TiO₂ NPs. The decrease in E_g with increasing thickness may be due to the possibility of structural defects, which in their rule lead to the formation of donor levels within the energy gap. These results were identical to those of Jagpreet *et al.*²⁹.

FTIR spectral studies

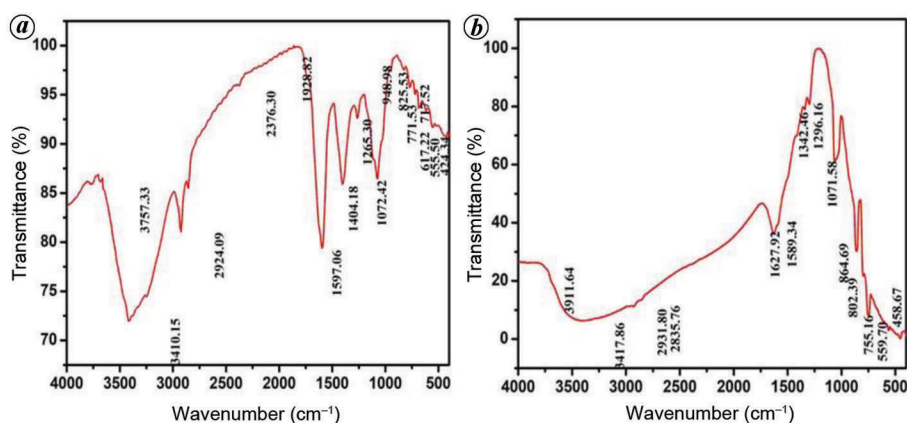
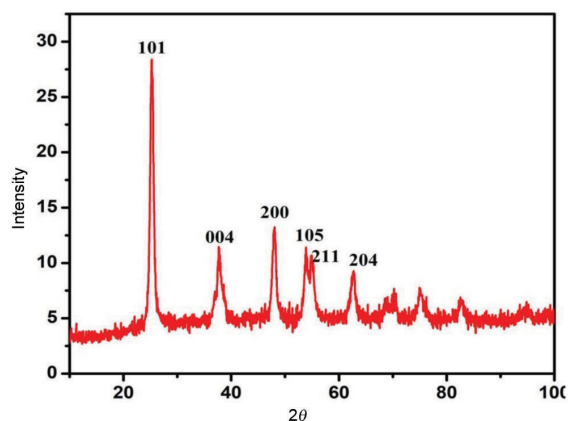
FTIR spectral analysis was carried out to identify the functional groups of molecules bound specifically along the surface of TiO₂ NPs. Figure 5 shows the FTIR spectra of green synthesized TiO₂ NPs and leaf powder of *E. variegata*. The spectrum was recorded in the range 4000–400 cm⁻¹. The peaks at 3418 and 1628 cm⁻¹ are due to O–H stretching and bending vibration of surface-adsorbed water respectively³⁰. This hydroxyl group bound to the surface of TiO₂ was assumed to trigger the photocatalytic activity of NPs. FTIR spectrum of green-synthesized NPs also showed characteristic bands at 2836 cm⁻¹, indicating the secondary amines and 2932 cm⁻¹ confirming the hydrogen-bonded alcohols. The strong peak noticed at 1589 cm⁻¹ represented aliphatic of the nitro compound with stretching of N–O and the peak at 1071 cm⁻¹ represented ethers. The absorption band with stretching mode of Ti–O in the fingerprint region 755 cm⁻¹, which corresponded to the anatase phase of TiO₂ (ref. 31). Thus, the FTIR results successfully confirmed the formation of anatase TiO₂, which is formed due to the reduction of TTIP precursor by phytochemical components present in the extract of *E. variegata* leaves. These components have several organic functional groups which attach to the surface of TTIP and cause a reduction of the same. Thus, they act as a good reducing as well as capping agents³².

X-ray diffraction studies

Figure 6 shows the XRD pattern of synthesized TiO₂ NPs. The peaks appearing at 2θ values of 25.28°, 37.82°, 48.01°, 53.89°, 55.03° and 62.64° correspond to the Bragg

Table 1. Structural and geometrical parameters of titanium dioxide (TiO₂)

Angle 2θ	Height (cts)	h k l	FWHM	d value (Å)	Relative intensity (%)
25.289	22.97581	1 0 1	0.76653	3.51891	100.0
37.829	4.96466	0 0 4	1.42267	2.37907	26.6
48.005	7.78938	2 0 0	0.94946	1.89436	34.0
53.897	5.42721	1 0 5	0.87328	1.69856	24.3
55.030	5.20181	2 1 1	1.03566	1.67297	20.8
62.641	3.8286	2 0 4	1.24493	1.36642	7.1

**Figure 5.** Fourier transform infrared spectra of (a) *Erythrina variegata* leaf extract and (b) TiO₂ NPs.**Figure 6.** X-ray diffraction pattern of TiO₂ NPs.

reflection of the (101), (004), (200), (105), (211) and (204) planes respectively. The above diffraction peaks indicate the tetragonal body-centred structure of TiO₂ NPs³³. Sharp and broad diffraction peaks were observed, which level the crystallinity and the nanosized crystallite. The data are in good agreement with JCPDS card no. 84-1285. The average size of TiO₂ NPs was calculated using the Debye-Scherrer equation.

$$D = K\lambda/\beta \cos \theta,$$

where D is the crystalline size under UV radiation, K the shape factor (0.9), λ the wavelength of X-rays (1.5406 Å), β the full width at half maximum and θ is the Bragg angle.

The maximum peak appeared at 2θ value of 25.28°, which corresponds to an average size of TiO₂ of 7.91 nm. Table 1 lists the structural and geometrical parameters of TiO₂ NPs.

Scanning electron microscopy

The morphological features of the synthesized TiO₂ NPs were studied by SEM analysis. SEM images confirmed that the synthesized TiO₂ NPs were tetragonal in shape. Figure 7 shows the physical morphology, particle size and aspect ratio of the synthesized NPs in the lowest and highest magnification of 20.00 and 50.00 kX respectively³⁴.

Energy-dispersive X-ray spectroscopy

The EDX spectrum of TiO₂ showed peaks for titanium (Ti), oxygen (O) and carbon (C) elements as well as the atomic and weight percentages. The observed peak of C was due to the presence of minerals in the *E. variegata* extract. This study confirms the active participation of *E. variegata* elements in the synthesis of TiO₂ NPs. It also supports the high purity of the synthesized sample³⁵. Figure 8 shows the EDAX results.

Photocatalytic activity of TiO₂ on methylene blue dye solution

In this study, methylene blue dye solution was degraded using green-synthesized TiO₂ NPs and UV irradiation (multi-lamp photo reactor at 365 nm). UV-Vis double-beam

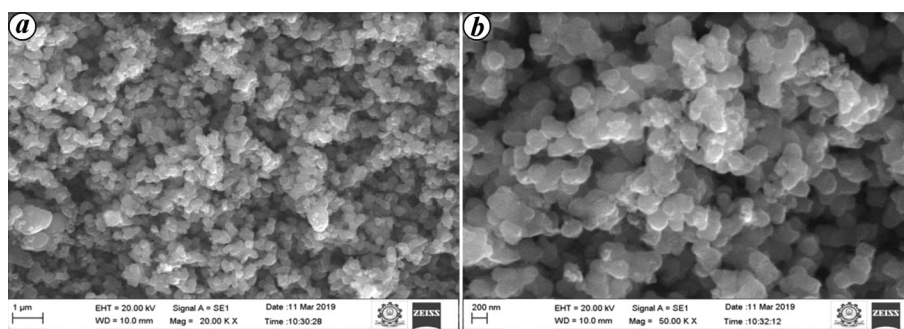


Figure 7. Scanning electron microscopic images of TiO₂ NPs.

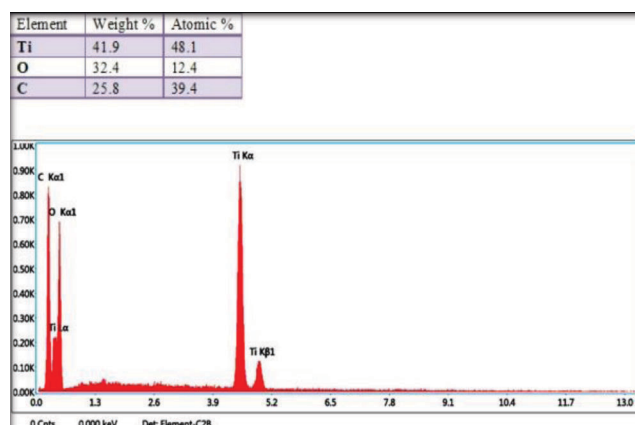


Figure 8. Energy-dispersive X-ray spectrum of TiO₂ NPs.

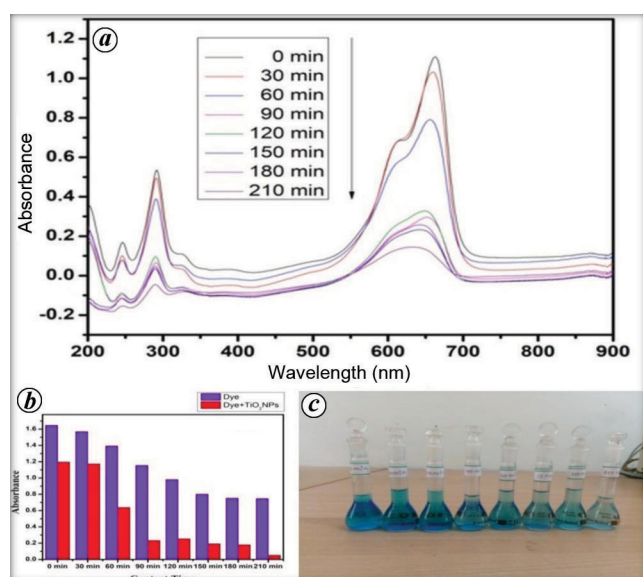


Figure 9. *a*, UV-Vis spectra of methylene blue dye degradation as a function of time. *b*, Variation of methylene blue dye degradation with and without TiO₂ NPs at different time intervals. *c*, Decolourization image.

spectrophotometer was used to measure absorbance of the dye solution before and after degradation at regular time intervals of exposure. Dye degradation was visually de-

tected by gradual change in the colour of the dye solution from deep blue to almost colourless. The characteristic absorption peak for methylene blue was noticed at 661 nm. The control exhibited no change in colour during exposure in the multi-lamp photo reactor (UV light source @ 365 nm). Degradation of the dye in the presence of TiO₂ NPs was verified by the decrease in peak intensity (at 661 nm) and the appearance of a new peak at 645 nm during 210 min of exposure. Figure 9 shows the optical density graph. The optimum absorbance peak of methylene blue dye observed at a wavelength of 661 nm decreased from 1.193 to 0.39. This in turn shows the tendency of the green-synthesized TiO₂ NPs to adsorb and degrade the pollutant. The formation of a new peak at 645 nm indicates that the chemical configuration of methylene blue dye starts to break up by UV-light. After 210 min under UV exposure the dye is found to degrade completely and effectively. When compared to the nano TiO₂ prepared from other plants extract³⁶.

Antibacterial activity of TiO₂ NPs

The antibacterial action of green-synthesized TiO₂ NPs was examined for four different pathogenic strains (*Streptococcus*, *Staphylococcus*, *E. coli* and *P. aeruginosa*). Using the disk diffusion method, zones of inhibition for Gram-positive and Gram-negative bacteria were found to be 7, 2, 8 and 14 mm in Figure 10. The results reveal that TiO₂ NPs synthesized using *E. variegata* leaves showed maximum antibacterial activity against *P. aeruginosa* compared to the other bacteria^{37,38} in Table 2.

Conclusion

The present study focuses on the green-synthesis of a transition metal of TiO₂ NPs using *E. variegata* leaf extract. The formation of NPs was confirmed by a colour change of the precipitate from pale yellow to sandal colour. It exhibited the maximum absorbance at 317.6 nm in UV spectral data. *E. variegata* leaf extract plays a prominent role in reducing TTIP to TiO₂ NPs. The energy-band gap of

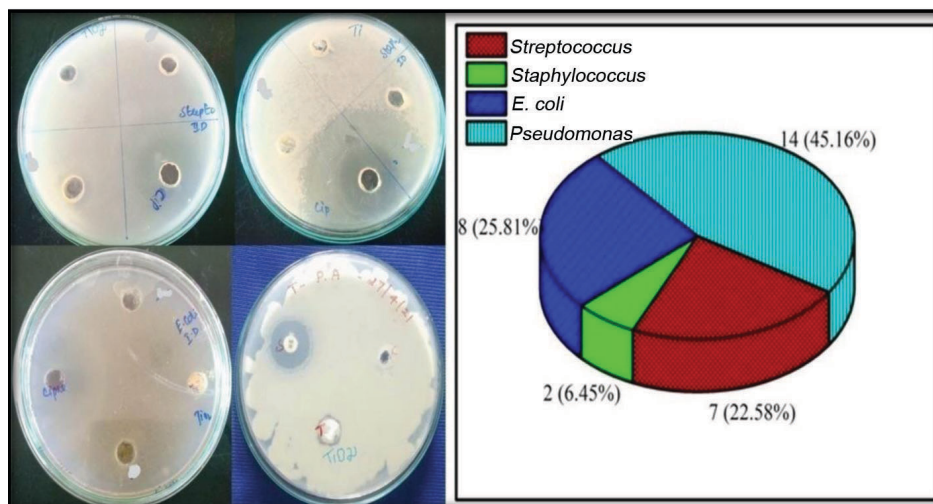


Figure 10. Well diffusion assay to assess bactericidal potential of biosynthesized TiO₂ NPs prepared from *Erythrina variegata* leaf extract against various bacterial strains, viz. *Streptococcus*, *Staphylococcus*, *Staphylococcus aureus*, *Escherichia coli* and *Pseudomonas aeruginosa*. Bar graph represents antibacterial activity.

Table 2. Antibacterial activity of TiO₂ NPs using *Erythrina variegata* leaf extract against pathogens

Name of organism	Zone of inhibition (mm)
<i>Streptococcus</i>	7
<i>Staphylococcus</i>	2
<i>Escherichia coli</i>	8
<i>Pseudomonas aeruginosa</i>	14

the synthesized TiO₂ NPs was found to be 2.35 eV by Tauc plots. FTIR studies confirmed that the functional groups associated with these were responsible for the formation of TiO₂ NPs. Structural properties of the synthesized NPs were studied by XRD analysis. The anatase phase TiO₂ sample having a tetragonal structure with a mean crystalline size was found to be 7.91 nm, which was calculated by the Debye–Scherrer equation. The tetragonal particle structure was observed in SEM image. The concentration of elements Ti and O maxima was calculated by EDAX analysis. The above results support that the green synthesis methodology is ideal for the synthesis of TiO₂ NPs. It is also a cost-effective and successful method. The NPs exhibit high photocatalytic activity, with promising applications in wastewater treatment of industrial dye methylene blue. They also act as an efficient bactericidal agent against Gram-positive and Gram-negative bacterial strains.

Conflict of interest: The authors declare that they have no conflict of interest.

1. He, J., Kunitake, T. and Nakao, A., Facile *in situ* synthesis of noble metal nanoparticles in porous cellulose fibers. *Chem. Mater.*, 2003, **15**, 4401–4406.
2. Cai, J., Kimura, S., Wada, M. and Kuga, S. and Nanoporous cellulose as metal nanoparticles support. *Biomacromolecules*, 2009, **10**, 87–94.

3. Jia, B., Mei, Y., Cheng, L., Zhou, J. and Zhang, L., Preparation of copper nanoparticles coated cellulose films with antibacterial properties through one-step reduction. *Appl. Mater. Interfaces*, 2012, **4**, 2897–2902.
4. Sastry, M., Ahmad, A., Islam Khan, M. and Kumar, R., Biosynthesis of metal nanoparticles using fungi and actinomycete. *Curr. Sci.*, 2003, **85**(2), 162–170.
5. Vainio, U., Pirkkalainen, K., Kisko, K., Goerigk, G., Kotelnikova, N. E. and Serimaa, R., Copper and copper oxide nanoparticles in a cellulose support studied using anomalous small-angle X-ray scattering. *Eur. Phys. J. D*, 2007, **42**, 93–101.
6. Rajender Reddy, K., Kumar, N. S., Sreedhar, B. and Lakshmi Kantam, M., *N*-Arylation of nitrogen heterocycles with aryl halides and arylboronic acids catalyzed by cellulose supported copper(0). *J. Mol. Catal. A*, 2006, **252**, 136–141.
7. Olsson, R. T. *et al.*, Making flexible magnetic aerogels and stiff magnetic nanopaper using cellulose nanofibrils as templates. *Nature Nanotechnol.*, 2010, **5**.
8. Liu, S., Zhou, J., Zhang, L., Guan, J. and Wang, J., Synthesis and alignment of iron oxide nanoparticles in a regenerated cellulose film. *Macromol. Rapid Commun.*, 2006, **27**, 2084–2089.
9. Tamayo, L., Azócar, M., Kogan, M., Riveros, A. and Páez, M., Copper-polymer nanocomposites: an excellent and cost-effective biocide for use on antibacterial surfaces. *Mater. Sci. Eng. C*, 2016, **69**, 1391–1409.
10. Das, S. K. and Mandal, A. B., Green synthesis of nanomaterials with special reference to environmental and biomedical applications. *Curr. Sci.*, 2015, **108**(11), 1999–2002.
11. Imran Din, M. and Aneelrani, Recent advance in the synthesis and stabilization of nickel and oxide nanoparticles. *Int. J. Anal. Chem.*, 2016, **4**, 14.
12. Kehinde, S., Enock, D., Adebayo, L. and Neerish, R., Biosynthesis, characterization and material applications of gold, silver, and palladium nanoparticles using aqueous extract of basella alba leaves. *Pac. J. Sci. Technol.*, 2016, **17**, 170–174.
13. Farzaneh, A., Mohammad, H. and Sara, S., Green synthesis of palladium nanoparticles using chlorella vulgaris. *Particles Lett.*, 2017, **186**, 113–115.
14. Rajoriya, P., Misra, P., Shukla, P. K. and Ramteke, P. W., Light-regulatory effect on the phytosynthesis of silver nanoparticles using aqueous extract of garlic (*Allium sativum*) and onion (*Allium cepa*) bulb. *Curr. Sci.*, 2016, **111**(8), 1364–1368.

15. Thangavelu, R. M., Munisamy, B. and Krishnan, K., Effect of deoxycholate capped silver nanoparticles in seed dormancy breaking of *Withania somnifera*. *Curr. Sci.*, 2019, **116**(6), 952–958.
16. Dinker, P., Shahista, S., Deshmukh, S. and Rohini, K., Green synthesis of copper nanoparticles using *Gloriosa superba* leaf extract. *Int. J. Pharma. Pharmac. Res.*, 2017, **12**, 203–209.
17. Pavan, G., Nagarajugoud, M., Kalyani, S., Shireesh, P., Madhuri, M., Srikar, N. and Abilash, M., Novel approach of condiment extract synthesis of nickel nanoparticles for antimicrobial activities: a green expertise. *Int. J. Adv. Res.*, 2016, **4**, 842–846.
18. Jayalakshmi and Yogamoorthi, A., Green synthesis of copper oxide nanoparticles using aqueous extract of flowers of *Cassia alata* and particles characterization. *Int. J. Nanomater. Biostruct.*, 2014, **4**, 66–72.
19. Jagpreet, S., Tanushree, D., Ki-hynu, H., Mohit, R. and Pallabi, S., Green synthesis of metals and their oxide nanoparticles for environmental remediation. *J. Nanobiotechnol.*, 2018, **16**, 1–50.
20. Amarnath, K., Saveetha, D. and Senniyanallur, R., Green synthesis and characterization of palladium nanoparticles and its conjugates from *Solanum trilobatum* leaf extract. *Nano-Micro Lett.*, 2010, **2**, 169–176.
21. Mujeeb, K., Merajuddin, K., Mufsir, K. and Syed, F., Biogenic synthesis of palladium nanoparticles using *Pulicaria glutinosa* extract and their catalytic activity towards the Suzuki coupling reaction. *Dalton Trans.*, 2014, **43**, 9026–9031.
22. Sundaramurthy, N. and Parthiban, C., Biosynthesis of copper oxide nanoparticles using *Pyrus pyrifolia* leaf extract and evolve the catalytic activity. *Int. Res. J. Eng. Technol.*, 2015, **2**(6), 332–338.
23. Vivek, P. and Preeti, J., Green synthesis of TiO₂ nanoparticle using *Morinda oleifera* leaf extract. *Int. Res. J. Eng. Technol.*, 2012, **4**, 3.
24. Santhoshkumar, T. and Rahuman, A., Green synthesis of titanium dioxide nanoparticles using *Psidium guajava* extract and its antibacterial and antioxidant properties. *Asian Pac. J. Trop. Med.*, 2014, **8**, 968–976.
25. Manish, H., Shreeram, J. and Mayur, D., Green synthesis of TiO₂ nanoparticles using aqueous extract of *Jatropha curcas* L. latex. *Mater. Lett.*, 2012, **75**, 196–199.
26. Tong, Z. and Shang, P., The stability electronic structure and optical property of TiO₂ polymorphs. *J. Phys. Chem.*, 2014, **118**, 11385–11396.
27. Saravanan, P., Ganapathy, M., Charles, A., Tamilselvan, S. and Vimalan, M., Electrical properties of green synthesized TiO₂ nanoparticles. *Pelagia Res. Lib.*, 2013, **7**, 158–168.
28. Ganesh, B., Mahendran, D., Indrarajselvi, P., Elangovan, N., Geetha, N. and Venkatachalam, P., Green engineering of titanium dioxide nanoparticles using *Ageratina altissima* King and H. E. Robbins medicinal plant aqueous leaf extracts for enhanced photocatalytic activity. *Ann. Phyomed.*, 2016, **5**, 2393–9885.
29. Jagpreet, S., Tanushree, D., Ki-Hynu, H., Mohit, R. and Pallabi, S., Green synthesis of metals and their oxide nanoparticles for environmental remediation. *J. Nanobiotechnol.*, 2018, **16**, 1–50.
30. Pawar, D., Shahista, S., Deshmukh, S. and Kanawade, R., Green synthesis of copper nanoparticles using *Gloriosa superba* leaf extract. *Int. J. Pharam. Pharam. Res.*, 2017, **12**, 203–209.
31. Senthilkumar, S., Ashok, M., Kashinath, L., Sanjeeviraja, C. and Rajendran, A., Phytosynthesis and characterization of TiO₂ nanoparticles using diospyros ebenum leaf extract and their antibacterial and photocatalytic degradation of crystal violet. *Smart Science*, Taylor & Francis, 2018, **6**(1), 1–9.
32. Kaur, H., Kaur, S., Singh, J., Rawat, M. and Kumar, S., Expanding horizon: green synthesis of TiO₂ nanoparticles using *Carica papaya* leaves for photocatalysis application. *Mater. Res. Express*, 2019.
33. Sethy, N. K., Arif, Z., Mishra, P. K. and Kumar, P., Green synthesis of TiO₂ nanoparticles from *Syzygium cumini* extract for photocatalytic removal of lead (Pb) in explosive industrial wastewater. *Green Process Syn.*, 2020, **9**, 171–181.
34. Ghalyb, M. Y., Jamila, T. S., El-Seesyc, I. E., Souayad, E. R. and Nasra, R. A., Treatment of highly polluted paper mill wastewater by solar photocatalytic oxidation with synthesized nano TiO₂. *Chem. Eng. J.*, 2011, **168**, 446–454.
35. Singh, G., Panday, S., Rawat, M., Kukkar, D. and Basu, S., Facile synthesis of CuO semiconductor nanorods for time-dependent study of dye degradation and bioremediation applications. *J. Nano Res.*, 2017, **46**, 154–164.
36. Dondaa, M. R., Kudlea, K. R., Alwala, J., Miryalaa, A., Sreedharb, B. and Rudraa, P., Synthesis of silver nanoparticles using extracts of *Securinega leucopyrus* and evaluation of its antibacterial activity. *Mater. Sci.*, 2013, **7**, 1–8.
37. Gnanasundaram, I. and Velavan, S., Synthesis of copper oxide nanoparticles using leaf extract of *Cissus vitifolias* and evaluation of its antimicrobial activity. *J. Nat. Remedies*, 2020, **21**(8), 87–93.
38. Al-Faouri, A. M., Abu-Karmai, M. H. and Awwad, A. M., Green synthesis of copper oxide nanoparticles using *Bougainvillea* leaves aqueous extract and antibacterial activity evaluation. *Chem. Int.*, 2021, **7**(3), 155–162.

ACKNOWLEDGEMENTS. We thank the Science Instrumentation Centre (SIC) of The Standard Fireworks Rajaratnam College for Women, Sivakasi; and Research Centre Department of Chemistry, VHNSN College, Virudhunagar for providing the necessary facilities for sample analysis. We also thank the International Research Centre of Kalasalingam Academy of Research and Education, Krishnankoil for providing analytical facilities.

Received 27 February 2020; revised accepted 4 May 2020

doi: 10.18520/cs/v123/i1/59-66